Texture and microhardness of Mg-Rare Earth (Nd and Ce) alloys processed by high-pressure torsion

Yousf Islem Bourezg, Hiba Azzeddine, Thierry Baudin, Anne-Laure Helbert, Yi Huang, Djamel Bradai, Terence G. Langdon

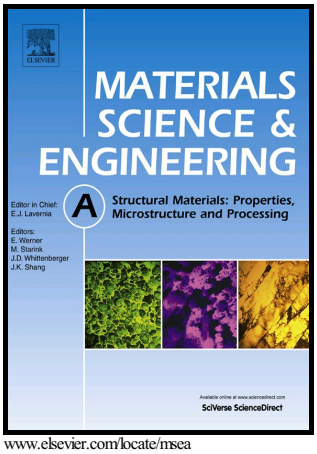

www.elsevier.com/locate/msea

PII: S0921-5093(18)30486-6
DOI: https://doi.org/10.1016/j.msea.2018.03.114
Reference: MSA36307

To appear in: *Materials Science & Engineering A*

Received date: 16 May 2017
Revised date: 14 January 2018
Accepted date: 28 March 2018

Cite this article as: Yousf Islem Bourezg, Hiba Azzeddine, Thierry Baudin, Anne-Laure Helbert, Yi Huang, Djamel Bradai and Terence G. Langdon, Texture and microhardness of Mg-Rare Earth (Nd and Ce) alloys processed by high-pressure torsion, *Materials Science & Engineering A*, https://doi.org/10.1016/j.msea.2018.03.114

Texture and microhardness of Mg-Rare Earth (Nd and Ce) alloys processed by high-pressure torsion

Yousf Islem Bourezg[a], Hiba Azzeddine[a,b*], Thierry Baudin[c], Anne-Laure Helbert[c], Yi Huang[d], Djamel Bradai[a], Terence G. Langdon[d]

[a] Faculty of Physics, USTHB, Algiers, Algeria.
[b] Department of Physics, University of M'sila, M'sila, Algeria.
[c]ICMMO, SP2M, Univ. Paris-Sud, Université Paris-Saclay, UMR CNRS 8182, 91405 Orsay Cedex, France
[d] Materials Research Group, Faculty of Engineering and the Environment, University of Southampton, Southampton SO17 1BJ, UK

[*]Corresponding author: azehibou@yahoo.fr

Abstract

The influence of high-pressure torsion (HPT) processing on the texture and microhardness of two binary Mg-RE (RE=Nd and Ce) alloys was investigated using X-ray diffraction and Vickers microhardness measurements. Disks cut from the alloys were processed by HPT at room temperature for up to 10 turns. The precipitation products of both alloys were identified using synchrotron radiation. The results show that both alloys exhibit a weak basal texture where the c-axis of most grains is shifted 15° from the shear direction. An Mg-1.44Ce (wt. %) alloy showed a continuous decrease in the texture strength which may be due to the effect of second precipitation phases ($Mg_{17}Ce_2$ and $MgCe_2$). The microhardness of both alloys increased significantly with increasing HPT turns but levelled-off beyond about one HPT turn. Maximum values of ~65 and ~96 Hv were achieved which are significantly higher than the hardness of the undeformed Mg-Ce and Mg-Nd alloys.

Keywords: Mg-Rare Earth alloy; High-Pressure Torsion; Microhardness; Twinning; Second phase; Texture.

1. Introduction

Despite their favorable thermal stability and strength, magnesium alloys have a disadvantage because of their poor room temperature formability and ductility which is caused by the basal texture in the microstructure and basal slip during deformation [1]. This disadvantage may be limited or even avoided through microstructural changes by the addition of alloying elements, through appropriate mechanical processing or combinations of both. A review of the literature indicates that additions of small amounts of rare earth (RE) elements, such as Nd, Ce, Y, Gd and La, provide the potential for improving the room temperature formability, modifying the recrystallization kinetics and the plastic deformation behavior as well as influencing the texture evolution of Mg-based alloys [2–10].

It has been reported that, contrary to conventional Mg-based alloys with non-RE elements, either small (Mg-X (X=Nd, Ce, Y, La)) or heavy additions of RE (WE alloys) can develop more random-type texture during deformation processing [10–13]. It was suggested that the modified texture in Mg-RE alloys was due to particle-stimulated nucleation of recrystallization (PSN) following deformation [11]. Nerveless, PSN is not the single mechanism responsible for RE-texture modification, especially in the case of Mg-based alloys containing RE micro-alloying with a very small amount of second phase. The promotion of non-basal slip such as <a> prismatic and/or <c + a> pyramidal slip via a solute strengthening mechanism and the suppression of grain boundary mobility through solute drag were proposed as solid solution-based mechanisms responsible for the texture weakening in Mg-RE alloys [13–15].

The mechanical processing of metals through the application of intense deformation provides the potential for achieving significant grain refinement [16]. Specifically, severe plastic deformation (SPD) techniques, such as equal-channel angular pressing (ECAP) [17], accumulative roll bonding (ARB) [18] and high-pressure torsion (HPT) [19, 20], have the

capacity to produce ultrafine-grained (UFG) microstructures [21–23] and also significantly affect the size/distribution of precipitates within the crystalline matrix [24].

It is well known that processing of metals through the application of intense deformation provides a potential for achieving important additional microstructural modifications such as very high dislocation densities and high densities of point defects [16].

To date, many available scientific reports demonstrate the successful achievement of grain refinement down to the sub-micrometer level and significant improvements of the mechanical properties in various Mg-based alloys processed by SPD techniques [25–28]. Frequently, SPD processing (such as by ECAP) of Mg-based alloys were performed at a relatively high temperature (200–300 °C) [29]. Consequently, the grain refinement was rather limited due to the occurrence of recovery and even dynamic recrystallization during processing. Surprisingly, the hydrostatic stresses developed during HPT processing prevented cracking and allowed the processing of magnesium alloys even at room temperature [30]. Moreover, it has been confirmed that HPT processing gave more significant grain refinement compared to ECAP processing of the same AZ31 alloy and at a similar temperature (200 °C) [31, 32].

The crystallographic texture of Mg-based alloys such as pure Mg, AZ31and ZK60A alloys after HPT processing was characterized by a basal texture where the *c*-axis rotates from the disc plane towards the torsion axis [33–36]. The deviation of the *c*-axis from the torsion axis depends strongly on the HPT processing temperature [36]. Detailed texture analysis revealed a significant difference in the evolution of texture between the overall texture taken throughout the disk and the local texture at the disk edges up to 5 HPT turns [34, 35].

The microstructures and thermal stability of an Mg-Gd alloy processed by HPT were investigated using positron annihilation spectroscopy (PAS) and transmission electron microscopy (TEM) [37, 38]. The results showed that the Mg-Gd alloy exhibited a

homogeneous UFG microstructure with a high density of uniformly distributed dislocations and a grain size of about 100 nm with a concomitant significant rise of hardness [37]. An appreciable thermal stability up to 300°C was also reported [38].

It was also demonstrated that HPT processing strongly affects the precipitation kinetics in Mg-RE alloys [39]. The occurrence of precipitation was shifted to a lower temperature in the HPT-deformed sample and this shift was associated with a high fraction of grain boundaries that act as potential nucleation site of a second phase and the enhanced difficulty of the solute elements to diffuse along grain boundaries [39].

To the present time, little information is available on the crystallographic texture and mechanical properties of Mg-RE alloys subjected to HPT processing [33] and this contrasts with the extensive published data about Mg-based alloys subjected to conventional deformation [40–45]. Accordingly, the objective of the present research was to investigate the influence of HPT processing at room temperature on the texture and the microhardness of two Mg-RE alloys (Mg-1.43Nd and Mg-1.44Ce (wt. %)) in the presence of precipitates and residual solute elements.

2. Experimental materials and procedure

The materials used in this investigation were alloys of Mg-1.43Nd and Mg-1.44Ce (wt.%) supplied in an as-cast state by colleagues from the Institutfür Metallkunde und Metallphysik (IMM), Aachen, Germany. Discs with diameter of 10 mm were machined from the as-cast materials and then homogenized in sealed glass tubes at 535 °C for 5 h.

After homogenization, disks with thicknesses of 1.5 mm were sliced from the cylindrical samples and then carefully polished with abrasive papers to final thicknesses of ~0.85 mm. The HPT processing was conducted at room temperature with a rotational speed of 1 rpm up to 1/2, 1, 5 and 10 turns using an imposed pressure of 6.0 GPa. All disks were

processed by HPT under quasi-constrained conditions [46] where there is a limited out-flow of material around the periphery of the disk during processing.

The textures were determined at the centers and edges of the disks processed by HPT by measuring the incomplete pole figures using a Phillips X-ray texture goniometer. A set of six measured pole figures $\{10\bar{1}0\}$, $\{0002\}$, $\{10\bar{1}1\}$, $\{10\bar{1}2\}$, $\{11\bar{2}0\}$ and $\{10\bar{1}3\}$ was used to calculate the orientation distribution function using the MTEX toolbox [47]. Figure 1 shows a representation of the axis system to assist the texture representation, where SD, RD and CD refer to the shear, rotation and compression directions, respectively.

X-rays diffraction patterns were obtained using the high photon flux synchrotron X-ray beam at MaxLab, Lund, Sweden (beamline I711). A wavelength of 0.9938 Å was calibrated using a Si (111) single-crystal monochromator. A large area Titan CCD detector from Agilent with a radius of 165 mm was used in the range 12–60° in 2θ. The volume fraction of precipitates was determined from a quantitative analysis using MAUD (for Material Analysis Using Diffraction, http://www.ing.untin.it/ ~luttero/) software.

The Vickers microhardness was measured on the cross-section in the center and edge of the deformed disk. At least five indentations were recorded to obtain the average hardness values with a load of 100 g ($Hv_{0.1}$) and dwell time of 10 s.

3. Experimental results

The microstructures of the solution-annealed Mg-1.43Nd and Mg-1.44Ce alloy are given in Fig. 2(a) and (b), respectively. Inspection shows that the microstructures of both alloys are characterized by elongated large columnar grains with average transverse grain sizes of ~ 400 μm. It was not possible to effectively characterize the initial texture due to the very poor statistics with records of only 22 grain orientations for Mg-1.43Nd and 13 grain

orientations for Mg-1.44Ce. Nevertheless, it is reasonable to assume that the texture is random.

The evolution of the texture measured at the center and edge of the HPT processed disks of both alloys are presented in Figs 3 and 4 in terms of the basal (0002) recalculated pole figures, respectively. As can be seen, the developed texture at the center and edge of the HPT processed disks of both alloys was globally similar and shows an asymmetric split of the basal planes shifted towards SD.

The intensity distributions of the basal (0002) poles of the processed Mg-1.43Nd and Mg-1.44Ce alloys are shown in Fig. 5 as a function of the polar angular tilt towards SD. It is readily apparent in Figs. 5(a) and 5(b) for Mg-1.43Nd that in the center and edge of the ½ turn HPT processed disks there are two intensity maxima around 15° and 40° shifts towards SD. However, the Mg.144Ce alloy after ½ HPT turn shows in both the center and edge of the HPT-processed disks a strong basal texture (~8.8 mrd) where the basal (0002) planes are parallel to the shear (SD, RD) plane or the c-axis is parallel to CD. From Figs. 5 (c) and (d), the basal maximum intensity is located at 15° towards SD. With increasing strain, the splitting shown in Mg-1.43Nd disappears and a basal texture appears. This basal texture is visible in the form of a crescent unilaterally shifted towards SD (15°) in the basal (0002) images of Figs 3 and 4. Figure 5 demonstrates clearly that all samples exhibit an asymmetric basal texture, with the distribution of the basal poles lying towards CD.

It is interesting to note that a similar texture evolution was reported in the WE54 alloy after hot uniaxial compression [44]. The present results show that the intensity of the basal texture of the Mg-1.43Nd alloy is essentially stable during HPT processing except after 5 HPT turn, as demonstrated in Fig. 3(c) and Figs. 5(a), 5(b) where the intensity increases to reach a maximum of 8.8 mrd in the edge of the 10 HPT sample. The Mg-1.44Ce alloy developed a similar type of basal texture in the center and edge of the sample, but the

intensity decreased continuously with increasing numbers of HPT turns from ~8.8 mrd after ½ HPT turn to ~ 4.2 mrd after 10 HPT turns in the center and from ~8.7 mrd after ½ HPT turn to ~5.6 mrd after 10 HPT turns in the edge. It is interesting to note that the texture in the center of the Mg-1.44Ce alloy is different after 10 HPT turns because symmetrical splitting of the weak basal poles is formed from CD towards SD and a new weak component also appears that is a basal (0002) pole 45° tilted from SD.

The 1D-XRD patterns from the high photon flux synchrotron for the HPT-processed Mg-1.43Nd and Mg-1.44 Ce alloys are shown in Fig. 6 after 1 and 10 turns. Inspection of these patterns shows that the use of a high beam easily reveals the different precipitate peaks that are often obscured in the background when using more conventional XRD techniques.

Figure 7 illustrates the microhardness evolution in the center and edge of Mg1.43Nd and Mg-1.44Ce HPT-processed disks with increasing numbers of HPT turns. Thus, the microhardness increases significantly in the initial stages with increasing HPT turns but after about 1 turn it essentially saturates for both alloys. The maxima values are ~65 and ~96 Hv for the Mg-Ce and Mg-Nd alloys and these values are ~57 and ~100 % more than the hardness values of the undeformed Mg-Ce and Mg-Nd alloys, respectively. From Fig.7, it can be seen also that the hardness as well as the hardening rate at the beginning of HPT for Mg-Nd are obviously higher than those for Mg-Ce.

4. Discussion

4.1 Texture evolution

The texture results demonstrate that the Mg-1.44Ce alloy develops a weaker texture than the Mg-1.43Nd alloy during HPT processing. It is known that the Ce element exerts a stronger effect on texture and grain size compared to other RE elements such as Y and Gd and this is due to the strong Ce interaction with dislocations and grain boundaries [48].

Nevertheless, another investigation on the effect of RE elements (Ce, La, Nd, Gd) on the sheet texture modification during warm rolling of a ZEK 100 alloy showed that the Ce and Nd elements led to similar texture evolutions [49]. The texture weakening after addition of these RE elements is associated with the grain boundary pinning effects caused by solute segregation and precipitate particles and the suppression of twinning [50–52]. In this context, it is important to consider the effect of residual Nd and Ce solutes and possible precipitated Mg_xRE_y particles.

As is apparent from inspection of Fig. 6, the XRD patterns of the HPT-processed alloys show that the Mg-1.44Ce alloy contains large volume fractions, proportional to their intensities, of two second phases identified as $MgCe_2$ (space group I4/mmm, $a = b$= 1.036 nm and c = 0.596 nm) and $Mg_{17}Ce_2$ (space group P63/mmc, $a = b$= 1.035 nm and c = 1.026 nm). By contrast, smaller amounts of the $Mg_{12}Nd$ phase (space group I4/mmm, $a = b$ = 1.031 nm and c = 0.593 nm) exist in the Mg-1.43Nd alloy as shown in Fig. 6(a) and (b). The volume fraction of precipitates determined from a quantitative analysis using MAUD software were as follows: Fv ($Mg_{17}Ce_2$) = 4–4.5 % and Fv ($Mg_{12}Nd$) = 1–1.5 % and obviously there was no variation upon straining. Additionally, a close inspection of the matrix (Mg) diffraction peaks revealed no shift of their 2θ angular positions.

Consequently, the heat treatment at 535 °C for 5 h failed to ensure a fully-homogenized solid solution in both alloys. From a close inspection of the precipitate peaks, it is concluded that more residual Nd atoms remain in the Mg-Nd alloy than Ce atoms in the Mg-Ce alloy.

It was reported that the presence of a large volume fraction of second-phase particles in the AZ91 alloy leads to weak deformation textures at high strains where this is attributed to the reduction of the twinning activity and the promotion of dynamic recrystallization [53]. However, the suppression or the activation of twining by interaction with particles depends

strongly on their size and their distribution within the microstructure [54–56]. For example, a particle spacing of ~100 nm was found to lead to the suppression of twins in Mg–1.62 Mn and Mg–5% Zn alloys [54, 55]. Unfortunately, in the present research the size and distribution of the $Mg_{17}Ce_2$, $MgCe_2$ and $Mg_{12}Nd$ second phases, as well as the Nd and Ce residual supersaturations in both alloys, are not known precisely. It is also worth noting that these characteristics may be strongly affected by the HPT processing. Moreover, in addition to the lack of direct evidences for the size and distribution of precipitates, it is not clear whether or not there is a suppression of twinning in the two alloys and whether the precipitates influence the recovery and recrystallization. Consequently, it is believed that the texture difference between the two alloys may be partly due to the effect of second phase particles and residual solutes.

The texture evolutions of both alloys are different from the typical torsion texture where most of the (0002) planes of grains are oriented parallel to the shear (SD-RD) plane [57]. Furthermore, the texture in this investigation is different from that in other Mg-based alloys processed by HPT [34–36]. Indeed, the textures obtained are not only weaker in the Mg-RE alloy but also the qualitative characters of the textures were altered as well. For example, the texture of an AZ31 alloy after HPT processing at room temperature exhibited two fibres, a rotated basal texture (10° towards SD) and a second fibre (φ_1 = 87°, Φ = 68° and φ_2 = 0 to 60°) [36]. It was also found that the HPT processing temperature affects the angle between the c-axis and the torsion axis such that the c-axis is 10° from the torsion axis at 25 and 100 °C but 5° from the torsion axis at 200 °C [36]. For commercially pure Mg processed by HPT at room temperature up to 8 turns there was a typical torsion texture and it was stable after one HPT turn [34]. A weak basal fibre texture that saturated with increasing numbers of HPT turns (up to 5 turns) was reported in a ZK60A (Mg-6Zn-0.5Zr wt.% alloy) after HPT processing at room temperature [35].The formation of a typical torsion texture was attributed

to the activation of $\{10\bar{1}2\}<10\bar{1}1>$tension twinning that caused a rotation of the basal planes about 86.3° to SD [34]. During further HPT processing, and since the grains are now oriented in positions where dislocation slip on basal <a> or prismatic <a> planes may dominate over the twinning, the c-axis became perpendicular to SD and the Schmid factor of <a> dislocation slip was not zero.

It is well known that the deformation texture depends strongly on the initial texture of the alloy with respect to the loading and torsional plane [35]. The initial texture was assumed random in the present investigation. For this situation, the c-axis of the grains may be parallel, perpendicular or may have any orientation relatively to SD, so that the basal <a>, prismatic <a> and/or pyramidal <c + a> slip can be activated and probably contribute to the torsional deformation during HPT processing [36]. The rare earth content in the Mg may also contribute to the activation of non-basal slip by modifying the stacking-fault energy (SFE) of the Mg matrix [58].

The Nd and Ce elements may play a crucial role in the resulted texture after HPT processing and the precise role of rare earth elements was investigated for the texture modification of Mg alloys [58]. It was assumed that the slow diffusivity of the rare earth elements in magnesium, together with the segregation of RE element on the grain boundaries and dislocations, will slow down the movement of grain boundaries and dislocations (solute drag) and hence this will influence the texture development during deformation [58]. The dominant part to texture weakening is, however, quiet difficult to determine. Moreover, it was reported that RE inter-metallic precipitates appear to be less effective than RE segregation to GBs or dislocations for producing texture modification.

There is also another factor which may explain the texture evolution during HPT at both the disk centers and edges but very little published information exists [36, 59]. This is associated with the deformation strain at the central region of the HPT disk that is very

complex, and varies with the position relative to the disk center. In the present study, the XRD macrotexture measurements were performed at the disk center and, unlike the disk edge, the sample texture was then complicated by the axial symmetric strain around the central axis.

4.2 Hardness evolution

The considerable increase in the hardness shown in Fig. 7 within 1/2 turn of HPT processing may be due not only to conventional dislocation and grain size hardening but also to texture strengthening. It is plausible that texture strengthening may play an important role in this early hardening during HPT where the strengthening is a direct consequence of the basal plane reorientations from a stochastic arrangement in the as-cast condition to an arrangement parallel to the shear direction (and thus vertical to the loading direction of the microhardness tests) [34].

Many authors have reported similar significant grain refinement within one HPT turn [34, 35, 60]. In addition, the very slight change between 1 and 10 HPT turns is due in part to a concomitant saturation of grain subdivision and the dislocation density and in part to a recovery of dislocations which begins even at room temperature in HPT-deformed Mg [61]. Values of the hardness achieved in this investigation are no more than 20 % higher than the peak age-hardening values reported for conventionally aged Mg-Ce and Mg-Nd alloys [62–67]. Furthermore, the microhardness evolution follows a trend that is similar to many metals processed by HPT or other SPD techniques [34, 66, 67]. The higher hardness and hardening rate at the beginning of the HPT processing observed for Mg-Nd by comparison with Mg-Ce may be associated with residual solute/dislocation and precipitate/dislocation effects as well as the concomitant influence of the complex Mg_xRE_y phase size, distribution and morphology. It is worth noting that there is very little if any data about such complex inter-correlations available in the literature and especially after severe plastic deformation.

As shown above, HPT processing neither induced a shift to lower angles (i.e. larger lattice parameter) for the α-Mg diffraction peaks nor decreased the intensities of the intermetallic diffraction peaks. Therefore, any dissolution of the $Mg_{12}Nd$ and $Mg_{17}Ce_2$ particles occurred upon increasing strain. Thus, the solute content of the α-Mg remains reasonably constant and causes no supplementary hardening. There is evidence for such solution hardening in an Mg-Gd-Y-Zn-Zr alloy after HPT processing [68]. Furthermore, this research also revealed a mechanism of dispersion hardening by which the Mg-RE intermetallics in the Mg-Gd-Y-Zn-Zr alloy were broken into small particles with sizes of ~1–10 μm and were then homogeneously dispersed in the matrix after HPT for 16 turns [68].

It is well known that metals and alloys strengthen through the four basic mechanisms of solid solution, precipitation, dislocation and grain boundary strengthening. Conventionally age-hardened Mg-RE alloys often exhibit a mixture of precipitate phases that have different morphologies, sizes and distributions. Then the overall strengthening of these alloys is totally determined by multi-form interactions between precipitates with dislocations and twins during the deformation process [65]. Basically, the strengthening is progressive up to the peak value and it is proportional to the volume fractions of the precipitates.

It is known that there are two main causes of hardening upon processing by SPD. These are the effects of a strong grain refinement which is accompanied by a steep evolution of the dislocation density [34]. However, these two effects may not apply in a simple manner in f.c.c metals owing to the simultaneous occurrence of recovery or dynamic recrystallization. In practice, it was shown that dynamic recrystallization leads to a bimodal distribution of small recrystallized grains embedded within the original large grains [30] and this development of a bimodal microstructure is fully consistent with the principles of grain refinement developed for Mg alloys processed by other SPD techniques [69, 70].

Earlier results showed that dynamic recrystallization takes place in the temperature range of approximately 147 – 327 °C for magnesium and its alloys that are usually processed by ECAP [71–74]. By contrast, in the present study the Mg-RE alloys were processed by HPT at room temperature and these conditions will probably prevent, or at least hinder, any dynamic recrystallization. A DSC analysis of the Mg-1.43Nd and Mg-1.44Ce alloys suggested that recrystallization may occur in the temperature range of ~180–220 °C. Moreover, it has been reported that defect recovery is stronger in Mg by comparison with Al, Cu, Ag and a range of metals with higher melting temperatures [34].

Finally, it is necessary to note that the presence of precipitate particles may also influence the defect recovery process and hence the overall hardening of the Mg-RE alloys. The processes of dislocation generation, recovery and the interaction of dislocations with precipitation products and the possibility of particle breakage are areas requiring further exploration. Nevertheless, the very weak evolution of hardness upon HPT processing between ½ and 10 turns appears to be due to a steady-state dislocation generation in work hardening and the annihilation or recovery of dislocations as proposed also in another report [75].

5. Summary and conclusions

- Mg-1.43Nd and Mg-1.44Ce alloys were processed by HPT at room temperature for up to 10 turns.
- The experimental textures at the centers and edges of the disks of both alloys were characterized by an asymmetric basal texture shifted 15° towards the shear direction with the appearance and disappearance of some minor components. The Mg-1.44Ce alloy developed a weaker texture than the Mg-1.43Nd alloy during HPT processing.

- Whereas for the Mg-1.43Nd alloy the texture was reasonably stable, there was a continuous decrease in the texture intensity in Mg-1.44Ce with increasing number of HPT turns and this was associated with the effect of $Mg_{17}Ce_2$ and $MgCe_2$ phases.
- The microhardness increased with increasing HPT turns but ultimately leveled off for both alloys.

Acknowledgements

DB gratefully acknowledges Dr. Olivier Balmes and Dr. Matej Zdeneck from Max IV synchrotron facility, Lund Sweden, for their kind invitation and assistance during his short stay. The work of two of us was supported by the European Research Council under Grant Agreement No. 267464-SPDMETALS (YH and TGL).

References

[1] S. Sandlobes, S. Zaefferer, I. Schestakow, S. Yi, R. Gonzalez-Martinez. On the role of non-basal deformation mechanisms for the ductility of Mg and Mg–Y alloys. Acta Mater. 59 (2011) 429–439.

[2] S. B. Yi, D. Letzig, K. Hantzsche, R. G. Martinez, J. Bohlen, I. Schestakow, S. Zaefferer. Improvement of magnesium sheet formability by alloying addition of rare earth elements. Mater. Sci. Forum 638-642 (2010) 1506–1511.

[3] K. Hantzsche, J. Bohlen, J. Wendt, K.U. Kainer, S.B. Yi, D. Letzig. Effect of rare earth additions on microstructure and texture development of magnesium alloy sheets. Scripta Mater. 63 (2010) 725–730.

[4] R. K. Mishra, A. K. Gupta, P. R. Rao, A. K. Sachdev, A. M. Kumar, A. A. Luo. Influence of cerium on the texture and ductility of magnesium extrusions. Scripta Mater. 59 (2008) 562–565.

[5] K. U. Kainer, J. Wendt, K. Hantzsche, J. Bohlen, S.B. Yi, D. Letzig. Development of the Microstructure and Texture of RE Containing Magnesium Alloys during Hot Rolling. Mater. Sci. Forum 654-656 (2010) 580–585.

[6] R. Cottam, J. Robson, G. Lorimer, B. Davis, in: A.D. Rollett (Ed.), Materials Processing and Texture, Wiley, Hoboken, NJ, USA (2008) 501.

[7] N. Stanford, D. Atwell, M.R. Barnett. The effect of Gd on the recrystallisation, texture and deformation behaviour of magnesium-based alloys. Acta Mater. 58 (2010) 6773–6783.

[8] Z. Liu, K. Zhang, X.Q. Zeng, The Theory Foundation of Magnesium- Based Lightweight Alloys and their Applications, Mechanical Industry Press, Beijing (2002) 52.

[9] N. Stanford, M.R. Barnett. The Origin of "Rare Earth" Texture Development in Extruded Mg-Based Alloy and Its Effect on Tensile Ductility. Mater. Sci. Eng. A 496 (2008) 399–408.

[10] N. Stanford, M. Barnett. Effect of composition on the texture and deformation behaviour of wrought Mg alloys. Scripta Mater. 58 (2008) 179–182.

[11] E.A. Ball, P.B. Prangnell. Tensile-compressive yield asymmetries in high strength wrought magnesium alloys. Scripta Metall. Mater. 31 (1994) 111–116.

[12] J. Bohlen, M.R. Nurnberg, J.W. Senn, D. Letzig, S.R. Agnew. The texture and anisotropy of magnesium–zinc–rare earth alloy sheets. Acta Mater.55 (2007) 2101–2112.

[13] L.W.F. Mackenzie, B. Davies, F.J. Humphreys, G.W. Lorimer. The deformation, recrystallisation and texture of three magnesium alloy extrusions. Mater. Sci. Technol. 23 (2007) 1173–1180.

[14] R. Cottam, J. Robson, G. Lorimer, B. Davis. Dynamic recrystallization of Mg and Mg–Y alloys. Crystallographic texture development. Mater. Sci. Eng. A 485 (2008) 375–382.

[15] J. P. Hadorn, K.Hantzsche, S. Yi, J. Bohlen, D.Letzig, J. A. Wollmershauser, S. R. Agnew. Role of solute in the texture modification during hot deformation of Mg-rare earth alloys. Metall. Mater. Trans. A 43 (2012) 1347–1362.

[16] R.Z. Valiev, R.K. Islamgaliev, I.V. Alexandrov. Bulk nanostructured materials from severe plastic deformation. Prog. Mater. Sci. 45 (2000) 103–189.

[17] R.Z. Valiev, T.G. Langdon. Principles of equal-channel angular pressing as a processing tool for grain refinement.Prog. Mater. Sci. 51 (2006) 881-981.

[18] Y. Saito, N. Tsuji, H. Utsunomiya, T. Sakai, R.G. Hong. Ultra-fine grained bulk aluminum produced by accumulative roll-bonding (ARB) process. Scripta Mater. 39 (1998) 1221–1227.

[19] N. A. Smirnova, V. I. Levit, V. I. Pilyugin, R. I. Kuznetsov, L. S. Davidova, V. A. Sazonova. Evolution of structure of fcc single crystals subjected to large plastic deformation. Phys. Met. Metall. 61 6 (1986) 127–134.

[20] A. P. Zhilyaev, T. G. Langdon. Using high-pressure torsion for metal processing: Fundamentals and applications. Prog. Mater. Sci. 53 (2008) 893–979.

[21] A. Y. Khereddine, F. HadjLarbi, H. Azzeddine, T. Baudin, F. Brisset, A.L. Helbert, M.H. Mathon, M. Kawasaki, D. Bradai, T. G. Langdon. Microstructures and Textures of a Cu-Ni-Si Alloy Processed by High-Pressure Torsion. J. Alloys Compds. 574 (2013) 361–367.

[22] K. Tirsatine, H. Azzeddine, T. Baudin, A-L Helbert, F. Brisset, B. Alili, D. Bradai.Texture and microstructure evolution of Fe-Ni alloy after Accumulative Roll Bonding. J. Alloys Compds. 610 (2014) 352–360.

[23] F. Hadj Larbi, H. Azzeddine, T. Baudin, M-H. Mathon, F. Brisset, A-L.Helbert, M. Kawasaki, B. Djamel, T. G. Langdon. Microstructure and texture evolution in a Cu-Ni-Si alloy processed by equal-channel angular pressing. J. Alloys Compds. 638 (2015) 88–94.

[24] J. Gubicza, I. Schiller, N.Q. Chinh, J. Illy, Z. Horita, T.G. Langdon. The effect of severe plastic deformation on precipitation in supersaturated Al–Zn–Mg alloys. Mater.Sci. Eng. A 460–461 (2007) 77–85.

[25] J. Bai, F.Xue, S. N. Alhajeri, T. G. Langdon. Microstructural Evolution of Mg-4Nd Alloy Processed by High-Pressure Torsion. Mater. Sci. Forum, 667-669 (2011) 391–396.

[26] Y. Estrin, S. B. Yi, H.-G. Brokmeier, Z. Zúberová, S. C. Yoon, H. S. Kim, R. J. Hellmig. Microstructure, texture and mechanical properties of the magnesium alloy AZ31 processed by ECAP. Int. J. Mater. Res. 99 (2008) 50–55.

[27] Z. Horita, K. Matsubara, K. Makii, T.G. Langdon. A two-step processing route for achieving a superplastic forming capability in dilute magnesium alloys. Scr. Mater. 47 (2002) 255–260.

[28] K. Matsubara, Y. Miyahara, Z. Horita, T.G. Langdon. Developing superplasticity in a magnesium alloy through a combination of extrusion and ECAP. Acta Mater. 51 (2003) 3073–3084.

[29] T. Mukai. M. Yamanoi, H. Watanabe, K. Higashi. Ductility enhancement in AZ31 magnesium alloy by controlling its grain structure. Scripta Mater. 45(2001) 89–94.

[30] R. B Figueiredo, M. T. P. Aguilar, P. R. Cetlin, T. G. Langdon. Processing magnesium alloys by severe plastic deformation. IOP Conf. Series: Mater. Sci. Eng. 63 (2014) 012171.

[31] P. Serre, R. B. Figueiredo, N. Gao, T. G. Langdon. Influence of strain rate on the characteristics of a magnesium alloy processed by high-pressure torsion. Mater. Sci. Eng. A 528 (2011) 3601–3608.

[32] R. B. Figueiredo, T. G. Langdon. Grain refinement and mechanical behavior of a magnesium alloy processed by ECAP. J. Mater. Sci. 45 (2010) 4827–4836.

[33] R. Kocich, L. Kuncicka, P. Kral, T. C. Lowe. Texture, deformation twinning and hardening in a newly developed Mg–Dy–Al–Zn–Zr alloy processed with high pressure torsion. Mater. Design 90 (2016) 1092–1099.

[34] X.G.Qiao, Y.W. Zhao, W.M.Gan, Y.C. Ming Y.Zheng, K. Wu, N.Gao, M.J. Starink, Hardening mechanism of commercially pure Mg processed by high pressure torsion at room temperature. Mater. Sci. Eng. A 619 (2014) 95–106.

[35] H.J. Lee, S.K. Lee, K.H. Jung, G.A. Lee, B. Ahn, M. Kawasaki, T.G. Langdon. Evolution in hardness and texture of a ZK60A magnesium alloy processed by high-pressure torsion. Mater. Sci. Eng. A630 (2015) 90–98.

[36] Y. Huang, R. B. Figueiredo, T. Baudin, A-L.Helbert, F. Brisset, T. G. Langdon. Microstructure and Texture Evolution in a Magnesium Alloy During Processing by High-Pressure Torsion. Mater. Res. 16 (2013) 577–585.

[37] J. Čížek, I. Procházka, B. Smola, I. Stulíková, R. Kužel, Z. Matěj,V. Cherkaska, R.K. Islamgaliev, O. Kulyasova. Microstructure and thermal stability of ultra-fine grained Mg and Mg-Gd alloys prepared by high-pressure torsion. Mater. Sci. Forum 482 (2005) 183–186.

[38] J. Čížek, I. Procházka, B. Smola, I. Stulíková, V. Očenášek, R. K. Islamgaliev, O. Kulyasova. Microstructure development and ductility of ultra-fine grained Mg-Gd alloy prepared by high pressure torsion. Mater. Sci. Forum 633-634 (2010) 353–363.

[39] J.Čížek, I.Procházka, B.Smola, I.Stulíková, M.Vlach, V.Očenášek, O. B. Kulyasova, R. K. Islamgaliev. Precipitation effects in ultra-fine-grained Mg–RE alloys. Int. J. Mater. Res. 100 (2009) 780–784.

[40] I. Basu, T. Al-Samman, G. Gottstein. Shear band-related recrystallization and grain growth in two rolled magnesium-rare earth alloys. Mater. Sci. Eng. A 579 (2013) 50–56.

[41] W. X. Wu, L. Jin, Z. Y. Zhang, W. J. Ding, J. Dong. Grain growth and texture evolution during annealing in an indirect-extruded Mg–1Gd alloy. J. Alloys. Compds. 585 (2014) 111–119.

[42] X. Xia, K. Zhang, X. Li, M. Ma, Y. Li. Microstructure and texture of coarse-grained Mg–Gd–Y–Nd–Zr alloy after hot compression. Mater. Design 44 (2013) 521–527.

[43] D. Elfiad, Y. I. Bourezg, H. Azzeddine, D. Bradai. Investigation of texture, microstructure, and mechanical properties of a magnesium-lanthanum alloy after thermo-mechanical processing. Int. J. Mater. Res. 107 (2016) 315–323.

[44] H. Azzeddine, D. Bradai. On the texture and grain growth in hot deformed and annealed WE54 alloy. Int. J. Mater. Res.11 (2012) 1351–1360.

[45] H. Azzeddine, D. Bradai. Texture and microstructure of WE54 alloy after hot rolling and annealing. Mater. Sci. Forum, 702-703 (2012) 453–456.

[46] R.B. Figueiredo, P.H.R. Pereira, M.T.P. Aguilar, P.R. Cetlin, T.G. Langdon. Using finite element modeling to examine the temperature distribution in quasi-constrained high-pressure torsion. Acta Mater. 60 (2012) 3190–3198.

[47] R. Hielscher, H.Schaeben. A novel pole figure inversion method: specification of the MTEX algorithm. J. Appl. Crystallogr. 41 (2008) 1024–1037.

[48] N. Stanford. Micro-alloying Mg with Y, Ce, Gd and La for texture modification—A comparative study. Mater. Sci. Eng. A 527 (2010) 2669–2677.

[49] T. Al-Samman, X. Li. Sheet texture modification in magnesium-based alloys by selective rare earth alloying. Mater. Sci. Eng. A 528 (2011) 3809–3822.

[50] J. Bohlen, D. Letzig, K.U. Kainer. New perspectives for wrought magnesium alloys. Mater. Sci. Forum 1 (2007) 546–549.

[51] T. Laser, Ch. Hartig, M.R. Nurnberg, D. Letzig, R. Bormann. The influence of calcium and cerium mischmetal on the microstructural evolution of Mg–3Al–1Zn during extrusion and resulting mechanical properties. Acta Mater. 56 (2008) 2791–2798.

[52] N. Stanford, S. Gang, A. Beer, S. Ringer, M.R. Barnett, in: Kainer, KU editor Magnesium: Proceedings of the 8th International Conference on Magnesium Alloys and Their Applications, 2009, DGM, Weimar, Germany. pp. 19–24.

[53] X. Li, F. Jiao, T. Al-Samman, S. GhoshChowdhury. Influence of second-phase precipitates on the texture evolution of Mg–Al–Zn alloys during hot deformation. Scripta Mater. 66 (2012) 159–162.

[54] N. Stanford, M. Barnett. Effect of composition on the texture and deformation behaviour of wrought Mg alloys. Scripta Mater. 58 (2008) 179–182.

[55] J.B. Clarke. Transmission electron microscopy study of age hardening in a Mg-5 wt.% Zn alloy. Acta Mater. 13 (1965) 1281–1289.

[56] C.J. McHargue, H.E. McCoy. Effect of interstitial elements on twinning in columbium. Trans. AIME 227 (1963) 1170.

[57] X.Q. Guo, W. Wu, P.D. Wu, H. Qiao, K. An, P.K. Liaw. On the Swift effect and twinning in a rolled magnesium alloy under free-end torsion. Scripta Mater. 69 (2013) 319–322.

[58] I. H. Jung, M. Sanjari, J. Kim, S. Yue. Role of RE in the deformation and recrystallization of Mg alloy and a new alloy design concept for Mg–RE alloys. Scripta Mater. 102 (2015) 1–6.

[59] R. B. Figueiredo, T. G. Langdon. Development of structural heterogeneities in a magnesium alloy processed by high-pressure torsion. Mater. Sci. Eng. A 528 (2011) 4500–4506.

[60] A. Y. Khereddine, F. HadjLarbi, M. Kawasaki, T. Baudin, D. Bradai, T. G. Langdon. An examination of microstructural evolution in a Cu–Ni–Si alloy processed by HPT and ECAP. Mater. Sci. Eng. A 576 (2013) 149–155.

[61] J. Cizek, I. Prochazka, B. Smola, I. Stulikova, R. Kuzel, Z. Matej, V. Cherkaska, R.K. Ismagaliev, O. Kulyasova. Defects in ultra-fine grained Mg and Mg-based alloys prepared by high pressure torsion studied by positron annihilation. Acta Phys. Polonica Series A, 107 (2005) 738–744.

[62] L.L. Rokhlin. Magnesium alloys containing rare earth metals, Taylor & Francis, New York (2003). p. 99

[63] K. Saito, H. Kaneki. TEM study of real precipitation behavior of an Mg–0.5at%Ce age-hardened alloy. J. Alloys Compds. 574 (2013) 283–289.

[64] C. Su, D. Li, T. Ying, L. Zhou, L. Li, X. Zeng. Effect of Nd content and heat treatment on the thermal conductivity of Mg–Nd alloys. J. Alloys Compds. 685 (2016) 114–121.

[65] J.F. Nie. Precipitation and hardening in magnesium alloys. Metall. Mater. Trans. A 43A (2012) 3891–3939.

[66] M. Kawasaki, H.J. Lee, B. Ahn, A.P. Zhilyaev, T.G. Langdon. Evolution of hardness in ultrafine-grained metals processed by high-pressure torsion. J. Mater. Res. Tech. 3 (2014) 311–318.

[67] K. Edalati, A. Yamamoto, Z. Horita, T. Ishihara. High-pressure torsion of pure magnesium: Evolution of mechanical properties, microstructures and hydrogen storage capacity with equivalent strain. Scripta Mater. 64 (2011) 880–883.

[68] W.T. Sun, C. Xu, X.G. Qiao, M.Y. Zheng, S. Kamado, N. Gao, M.J. Starink. Evolution of microstructure and mechanical properties of an as-cast Mg-8.2Gd-3.8Y-1.0Zn-0.4Zr alloy processed by high pressure torsion. Mater. Sci. Eng. A 700 (2017) 312–320.

[69] R.B. Figueiredo, T.G. Langdon. Principles of grain refinement in magnesium alloys processed by equal-channel angular pressing. J. Mater. Sci. 44 (2009) 4758–4762.

[70] R.B. Figueiredo, T.G. Langdon. The nature of grain refinement in equal-channel angular pressing: a comparison of representative fcc and hcp metals. Int. J. Mater. Res. 100 (2009) 1638–1646.

[71] S.E. Ion, F.J. Humphreys, S.H. White. Dynamic recrystallization and the development of microstructure during high temperature deformation of magnesium. Acta Metall. Mater. 30 (1982) 1909–1919.

[72] A. Galiyev, R. Kaibyshev, G. Gottstein. Correlation of plastic deformation and dynamic recrystallization in magnesium alloy ZK60. Acta Mater. 49 (2001) 1199–1207.

[73] M.M. Myshlyaev, H. J. McQueen, A. Mwembela, E. Konopleva. Twinning, dynamic recovery and recrystallization in hot worked Mg–Al–Zn alloy. Mater. Sci. Eng. A 337 (2002) 121–133.

[74] A.G. Beer, M.R. Barnett. Influence of initial microstructure on the hot working flow stress of Mg–3Al–1Zn. Mater. Sci. Eng. A 423 (2006) 292–299.

[75] B.B. Straumal, A. R. Kilmametov, Y. Ivanisenko, A. A. Mazilkin, O. A. Kogtenkova, L. Kurmanaeva, A. Korneva, P.Zieba, B. Baretzky. Phase transitions induced by severe plastic deformation: steady-state and equifinality. Int. J. Mater. Res. 106 (2015) 657–664.

Figure captions

Figure 1: Distribution of HPT-sample areas, where the texture measurements were performed. SD, RD and CD are corresponding to the shear, rotation and compression direction, respectively.

Figure 2: IPF maps showing the microstructure of annealed: a) Mg-1.43Nd and Mg-1.44Ce.

Figure 3: Basal (0002) recalculated pole figures near the centre and the edge of the disks of Mg-1.43Nd alloy proceeds by HPT at room temperature for: a) ½, b) 1, c) 5 and d) 10 turns.

Figure 4: Basal (0002) recalculated pole figures near the centre and the edge of the disks of Mg-1.44Ce alloy proceeds by HPT at room temperature for: a) ½, b) 5 and d) 10 turns.

Figure 5: Basal (0002) pole intensity distribution in shear direction (SD) of HPT deformed: a) near the centre, b) near the edge of the disks of Mg-1.43Nd, c) near the centre and d) near the edge of the disks of Mg-1.44Ce alloys.

Figure 6: XRD patterns of HPT deformed: Mg-1.43Nd alloy to a) 1 turn, b) 10 turns and Mg-1.44Ce alloy to c) 1 turn and c) 10 turns.

Figure 7: Evolution of Vickers microhardness with number of HPT turn of Mg-1.43Nd and Mg-1.44Ce alloys.

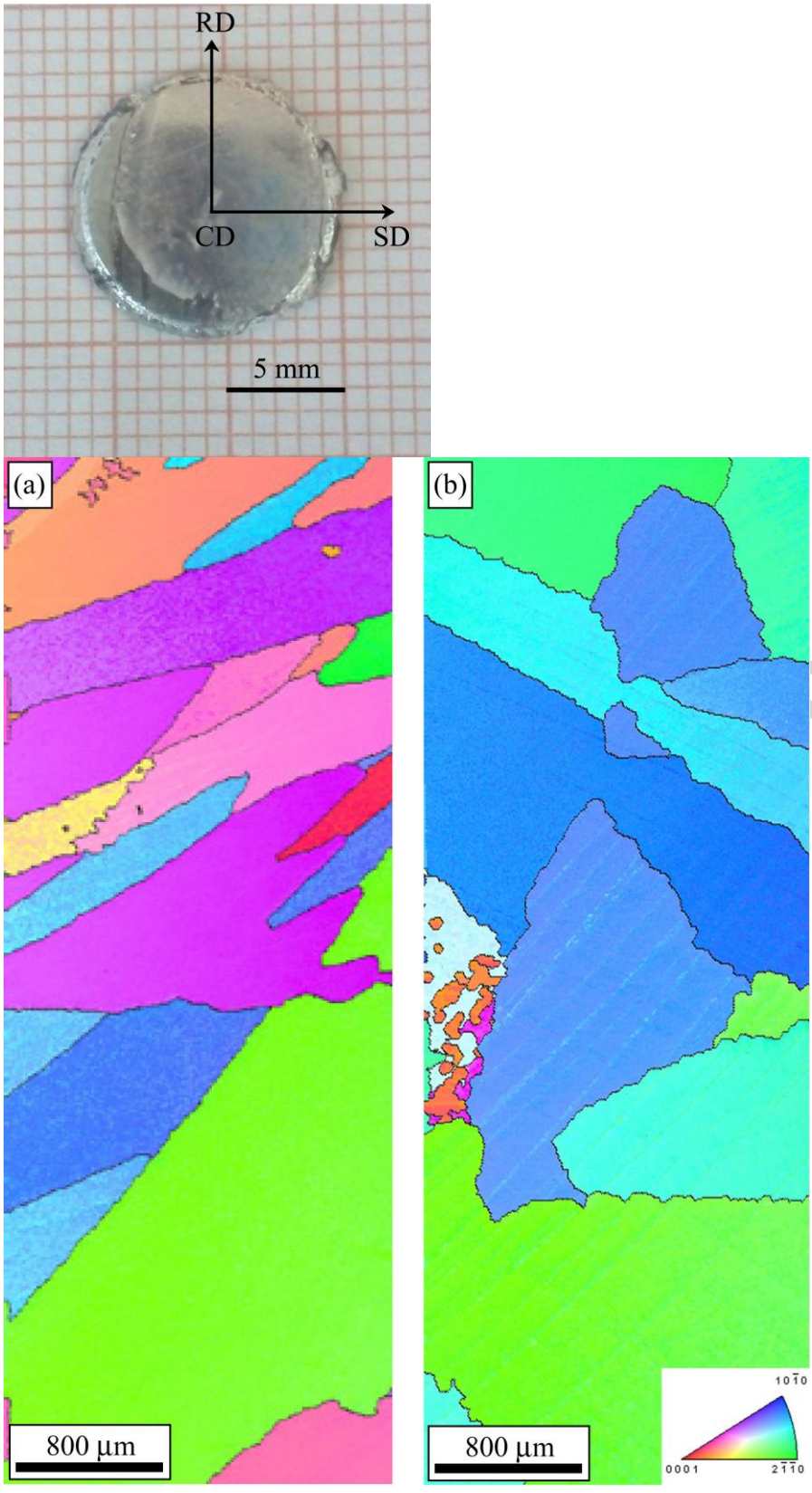
RD
CD
SD
5 mm
(a)
800 µm
(b)
800 µm
10$\bar{1}$0
0001
2$\bar{1}\bar{1}$0

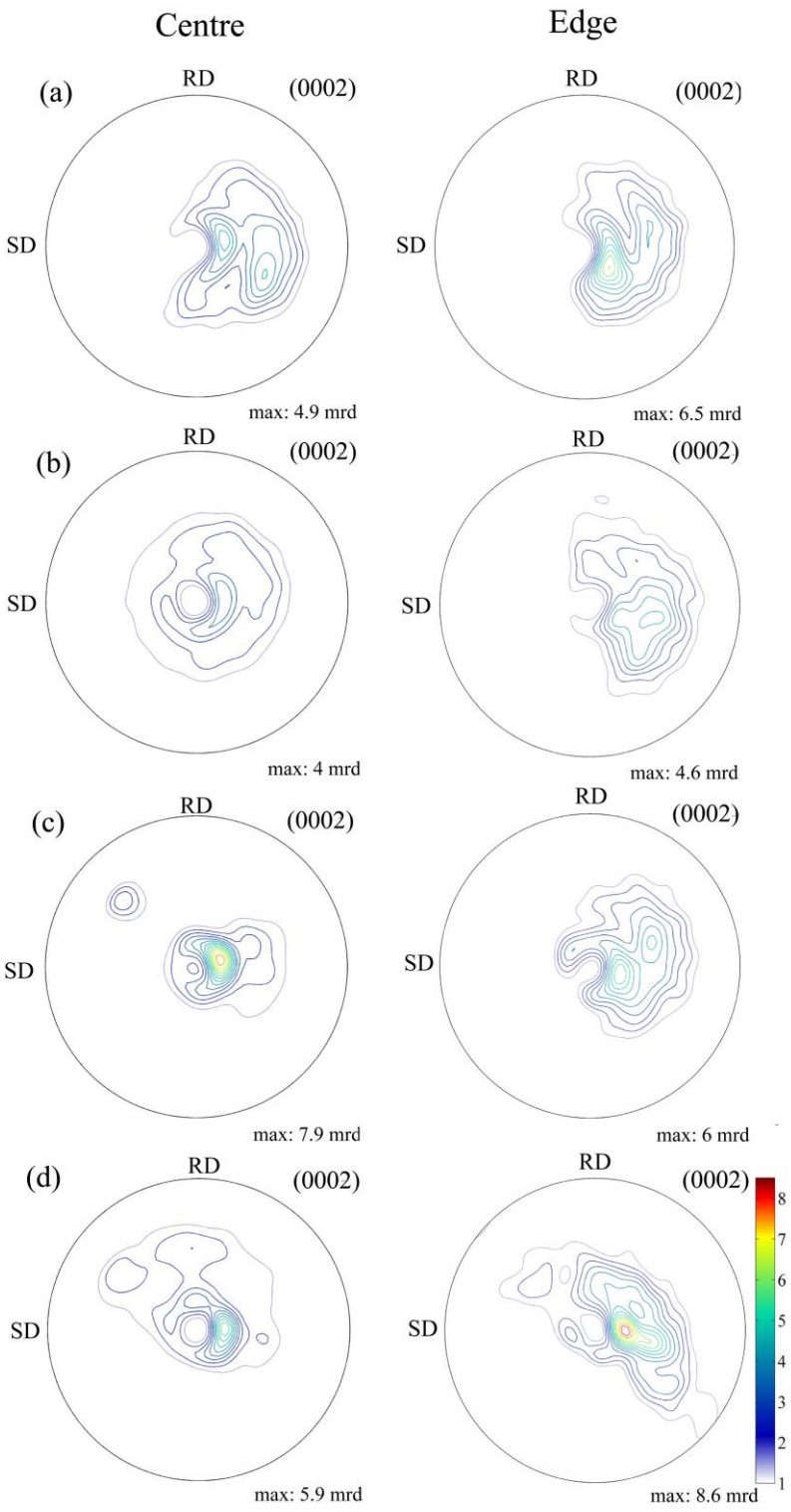
Centre
Edge
(a)
RD
(0002)
SD
max: 4.9 mrd
max: 6.5 mrd
(b)
max: 4 mrd
max: 4.6 mrd
(c)
max: 7.9 mrd
max: 6 mrd
(d)
max: 5.9 mrd
max: 8.6 mrd
8
7
6
5
4
3
2
1

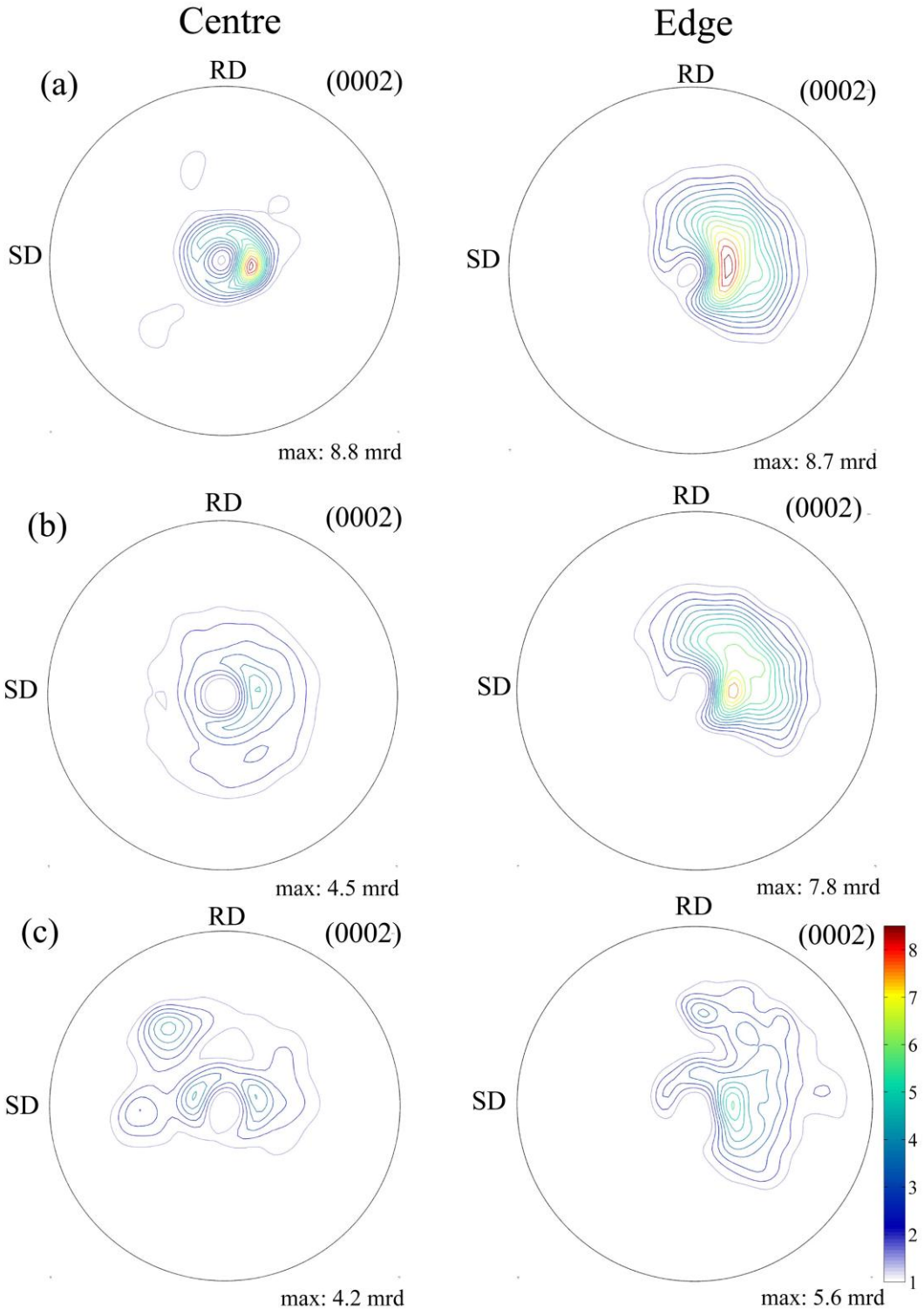
Centre
Edge
(a)
RD
(0002)
SD
max: 8.8 mrd
max: 8.7 mrd
(b)
max: 4.5 mrd
max: 7.8 mrd
(c)
max: 4.2 mrd
max: 5.6 mrd
8
7
6
5
4
3
2
1

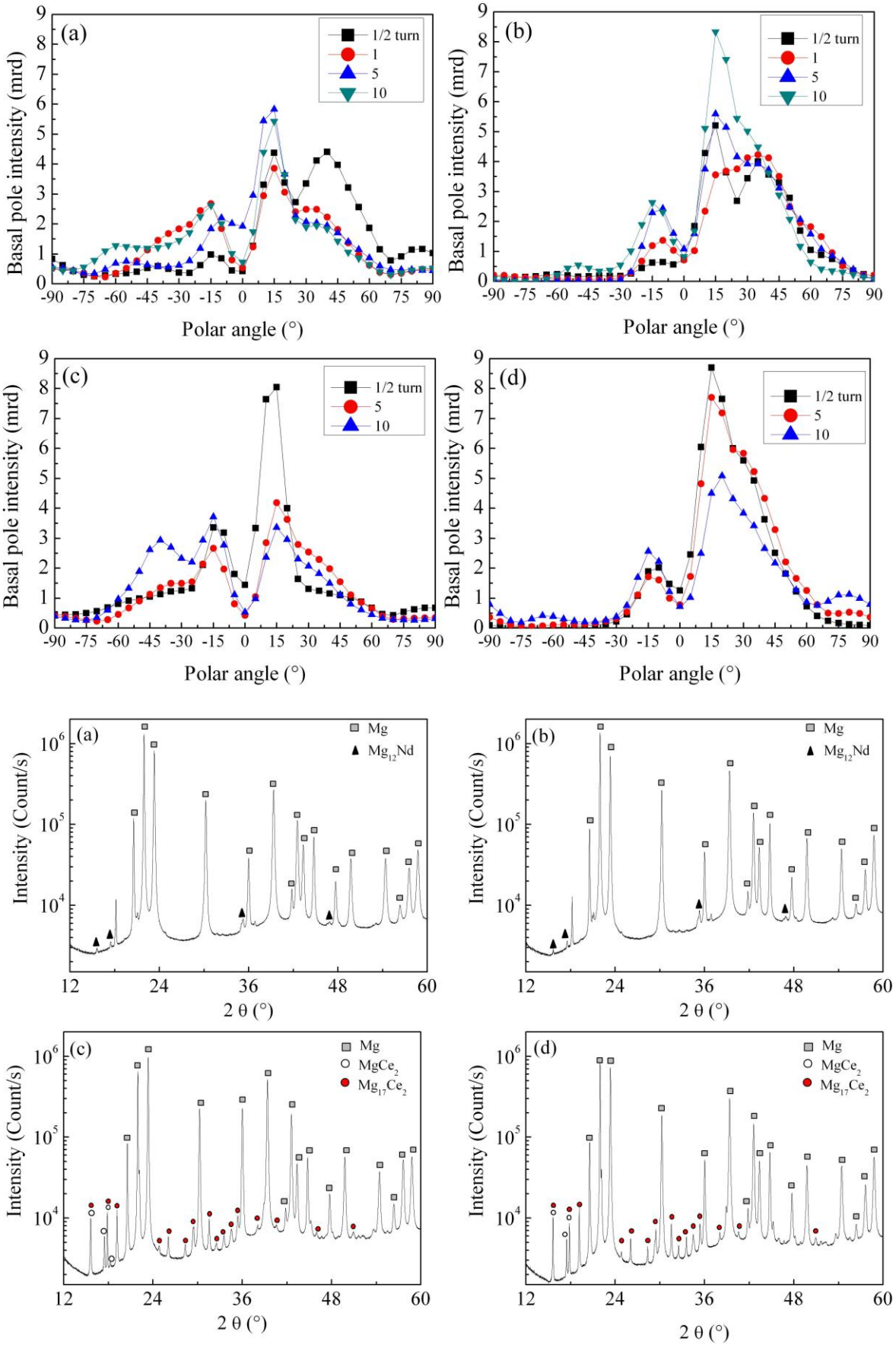
(a)
(b)
(c)
(d)
1/2 turn
1
5
10
Basal pole intensity (mrd)
Polar angle (°)
Mg
Mg12Nd
MgCe2
Mg17Ce2
Intensity (Count/s)
2 θ (°)